Irradiation-induced cellular senescence is linked to pro-survival signaling and checkpoint regulation in a 2D and 3D model for head and neck cancer

LUIS BUGIA[1*], ANNETTE AFFOLTER[1*], JOHANN KERN[1], EMMA SOHN[1], FREDERIC JUNGBAUER[1], JENS FLECKENSTEIN[2], ANNE LAMMERT[1], NICOLE ROTTER[1] and CLAUDIA SCHERL[1]

[1]Department of Otorhinolaryngology, Head and Neck Surgery, University Hospital Mannheim, Medical Faculty Mannheim of Heidelberg University, D-68167 Mannheim, Germany; [2]Department of Radiation Oncology, University Hospital Mannheim, Medical Faculty Mannheim of Heidelberg University, D-68167 Mannheim, Germany

Received November 12, 2024; Accepted May 14, 2025

DOI: 10.3892/or.2025.8984

Abstract. Fractionated irradiation causes premature senescence of tumor cells. Interactions between senescence, the immune system and survival signaling are poorly understood to date. As MAP kinases are implicated in immune resistance, the present study addressed the detection of senescence-associated modulation of postradiogenic programmed death-ligand 1 (PD-L1) and MAP kinase ERK1/2 expression in an *in vitro* and *ex vivo* model for head and neck squamous cell carcinoma (HNSCC). Established HNSCC cell lines (UM-SCC-11B, UM-SCC-14C and UM-SCC-22B) were employed to study the expression levels of p21, histone H2AX (γH2AX), PD-L1 and phosphorylated (p)ERK1/2 via immunohistochemistry following application of 4x2 Gy. Using senescence-associated β-galactosidase (SA-ß-Gal) staining, postradiogenic induction of senescence was additionally assessed. Results were validated in a 3D *ex vivo* HNSCC model with vital explants. Upon ionizing radiation (IR), senescence-like subpopulations were observed in all cell lines, showing upregulation of PD-L1 and pERK1/2 as well as of established senescence markers p21 and γH2AX. SA-β-Gal-positive cells were found in all lines. These results were supported in a 3D tumor model. Fractionated IR can generate a subpopulation of HNSCC cells characterized by senescence-typical cellular changes and marked expression of PD-L1 and pERK1/2. Postradiogenic senescence in both 2D and 3D cancer models was possibly related to survival signaling and immune checkpoint regulation, crucial elements in tumor development and progress.

Correspondence to: Professor Annette Affolter, Department of Otorhinolaryngology, Head and Neck Surgery, University Hospital Mannheim, Medical Faculty Mannheim of Heidelberg University, Theodor-Kutzer-Ufer 1-3, D-68167 Mannheim, Germany
E-mail: annette.affolter@umm.de

*Contributed equally

Key words: senescence, head and neck squamous cell carcinoma, programmed death-ligand 1, ERK1/2, p21, fractionated irradiation

Introduction

Senescent cells are characterized by a permanent cell cycle arrest, resistance to apoptosis and the bioactive secretion phenotype known as the senescence-associated secretory phenotype (SASP) (1-4). While cellular senescence has beneficial effects in early carcinogenesis and tumor therapy, studies have shown that the accumulation of senescent cells in age-related diseases, including cancer, has detrimental consequences. The persistence of these cells promotes cancer cell growth, aggressiveness and metastasis while contributing to an immunosuppressive tumor microenvironment (TME) (5,6). Previous research has highlighted the potential prognostic importance of senescent cells in HNSCC patients (7). The expression of SASP components has been linked to certain clinicopathological features, suggesting that senescence-related mechanisms may impact tumor progression and patient outcomes (8). Specific senescence-related genes hold prognostic value in HNSCC. For instance, a prognostic risk model incorporating these genes has been developed, offering potential as a biomarker for patient stratification and personalized treatment approaches (9). Cellular senescence can be effected by DNA damage caused by radiation therapy, which is one of the main treatment pillars in HNSCC. This therapy-induced senescence (TIS) contributes to tumor control by arresting the growth of cancer cells. However, the accumulation of senescent cells post-irradiation can also promote radioresistance. Early onset of senescence and the subsequent production of SASP factors have been identified as key determinants of this resistance in HNSCC (9).

The expression of radiation-induced senescence-associated genes has been suggested to have prognostic implications in HNSCC (10). Exposure to IR causes compensatory activation of intracellular signaling cascades securing tumor cell survival (11-13) such as signaling pathways MEK/ERK and PI3K/AKT in HNSCC (14,15). Our own previous studies

verify the IR-dependent induction of these cascades *in vitro* as well as in a 3D HNSCC *ex vivo* model most likely as a mechanism of resistance against radiotherapy (16-19). The response to therapeutic strategies in HNSCC is generally determined by a pronounced intratumorigenic heterogeneity (20) followed by a high variety in treatment response.

Immunotherapy has revolutionized treatment for a number of cancers including HNSCC over the past decade. In recurrent or metastatic HNSCC PD-1 inhibitors play an essential role (21,22). However, the majority of patients do not exhibit stable responses, suggesting the presence of mechanisms underlying *de novo* or acquired resistance to checkpoint inhibitors (CPI). Despite advances in the field, there remains a lack of robust biomarkers to predict clinical response and/or resistance to CPI (23).

Senescent cells have been shown to heterogeneously express the immune checkpoint molecule PD-L1 and that PD-L1+ senescent cells accumulate with age *in vivo*. In the context of potential anti-ageing therapy, the elimination of PD-L1+ senescent cells by immune checkpoint blockade has been described as a promising approach (24). Senescent cells upregulate PD-L1, the ligand for PD-1 on immune cells, leading to immune cell inactivation. Consequently, targeting PD-L1 has been proposed as a novel strategy for addressing senescence (25). Additionally, PD-L1 plays a role in the senescence of malignant cells via interferon-dependent cell cycle regulatory cascades or through its destabilization by cyclin D-CDK4 kinase (26-28). Notably, silencing PD-L1 in cancer cells has been shown to induce senescence (29). A potential link between checkpoint regulation and senescence is further supported by an investigation by Moreira *et al* (30), which investigated whether senescence markers could predict response to CPI in melanoma patients. Additionally, aging-related genes have been associated with chemotherapy resistance and linked to CPI response in HNSCC (7). Early senescence and the production of senescence-associated cytokines have also been identified as major determinants of radioresistance in HNSCC (9). Moreover, there is a notable connection between mitogen-activated protein kinase (MAPK) pathway activation and senescence. This relationship is exemplified by the association between MAPK ERK1/2 and p21, a key marker of senescence activation (31). Recently, we demonstrated a potential co-regulation of pERK1/2 and PD-L1 expression as a response to standard HNSCC treatment revealing a direct link between oncogenic drivers and PD-L1 expression (32).

Building on these findings, the present study used a 2D *in vitro* and a 3D *ex vivo* HNSCC model to map the effect of fractionated IR on the induction of senescence as well as its influence on checkpoint expression and survival signaling as part of a potential tumoral bailout mechanism.

Materials and methods

Cell culture. The cell lines UM-SCC-11B, UM-SCC-14C and UM-SCC-22B were obtained from Dr TE Carey (University of Michigan, Ann Arbor, MI, USA). Origins of the cell lines were larynx, oral cavity and hypopharynx, respectively (Table I) (33). Original tumors were not human papilloma virus-driven. The cells were cultivated in Dulbecco´s modified Eagle´s medium (DMEM; Thermo Fisher Scientific Inc.) supplemented with 10% fetal calf serum (FCS) and 1% penicillin/streptomycin (Gibco; Thermo Fisher Scientific Inc.). The authentication of all cell lines was confirmed by a recent Short Tandem Repeat (STR) profiling which is a DNA-based method used for authenticating and identifying cell lines (CLS Cell Lines Service GmbH; latest update Nov 2022).

Irradiation experiments. For each cell line, 200,000 cells/well were seeded in six-well plates and irradiated day 4 post-seeding on four consecutive days with a daily dose of 2 Gy using a linear accelerator (a device used in radiation therapy to deliver high-energy X-rays or electrons to tumors) with 6 megavolts (MV) photon energy (Elekta Synergy AB) and polymethylmethacrylate (PMMA) plates as water and tissue equivalents, respectively. Cells were left to recover again on days 8 and 9 and were harvested on day 10. Controls were mock-treated. Each experiment was performed three times (n=3).

Senescence-associated β-galactosidase (SA-β-Gal) staining. The cells were cultured in 9-well plates. After 48 h in culture, cells were irradiated with 2 Gy on four consecutive as aforementioned. Mock-treated samples served as controls. At 4 h after the last irradiation session, SA-ß-Gal staining was performed according to the manufacturer's instructions (Senescence β-galactosidase Staining Kit; cat. no. 9860; Cell Signaling Technology, Inc.). First, the growth medium was removed and the cells were washed once with 1X PBS. Then, 1 ml of 1X fixative solution was added to each 35 mm well and the cells were fixed for 10-15 min at room temperature (RT). After rinsing off the fixative solution with 1X PBS, 1 ml of the prepared β-galactosidase staining solution (comprising 930 μl of 1X Staining Solution, 10 μl of 100X Solution A, 10 μl of 100X Solution B and 50 μl of 20 mg/ml X-Gal) was added to each 35 mm well. The plate was sealed to prevent evaporation and incubated overnight at 37˚C in a dry incubator. The cells were then examined under the microscope (magnification, x200) for the development of blue staining. For long-term storage, the β-galactosidase staining solution was removed and the cells were overlaid with 70% glycerol. The plates were stored at 4˚C. The experiment was repeated three times.

Senescence induction was quantified by ImageJ software (National Institutes of Health, version 1.54p) and is given as relative amount of positive cells. Due to the small sample size normal distribution could not be assumed hence statistical assessment was performed using Mann Whitney U Test.

Immunohistochemical (IHC) staining. Cells were treated as described for SA ß-galactosidase staining and fixed by ice-cold ethanol/acetone (2:1) for 15 min on ice followed by treatment with antigen retrieval with Tris-EDTA buffer or Citrate buffer for antigen retrieval and subsequently endogenous peroxidase blockage with DAKO Peroxidase blocking solution (Agilent Technologies, Inc.). After preincubation with sheep normal serum 1:10 (BIOZOL Diagnostica Vertrieb GmbH) for 30 min at RT to avoid unspecific binding, primary antibodies [phosphorylated-p44/42 MAPK (Erk1/2; Thr202/Tyr204); cat. no. 9101 Cell Signaling Technology, Inc.; 1:400; PD-L1; cat. no. 13684, Cell Signaling Technology, Inc.; 1:400; p21 Waf1/Cip1 (12D1) Rabbit mAb cat. no. 2947, Cell Signaling Technology, Inc.; 1:500, Phospho-Histone H2A.X (Ser139;

Table I. Characteristics of the head and neck squamous cell carcinoma cell lines (33).

Characteristic	UM-SCC-11B	UM-SCC-14C	UM-SCC-22B
Specimen	Primary	Local recurrence	Lymph node metastasis
Tumor site	Larynx	Floor of mouth	Hypopharynx
TNM status	T2N2a	T2N0	T2N1
Previous therapy	CT	SU + CRT	None

CT, Chemotherapy; SU, Surgery; CRT, Chemoradiotherapy; TNM, Tumor, Node, Metastasis classification.

Table II. Characteristics of *ex vivo* specimens.

Fresh tissue sample	Patient 1	Patient 2	Patient 3	Patient 4
Patient age, sex	59, male	56, male	56, male	55, male
Tumor site	Oropharynx (Left Tonsil)	Oral cavity (Lower lip)	Larynx	Hypopharynx
TNM status	pT1 N0 M0	pT3 pN0 M0	rcT4a cN0 M0	pT4a pN2b M0
Histological risk factors	V0 L0 Pn0 R0 G2	V0 L0 Pn1 R0 G2	L0 V0 Pn0 G2	L1 V0 Pn1 R0 G3
Date (month/year) of sample collection	02/2024	05/2024	05/2024	06/2024

TNM, tumor, node, metastasis; V, Vascular invasion; L, Lymphatic invasion; Pn, Perineural invasion; R, Resection status; G, Grading.

20E3) Rabbit mAb cat. no. 9718, Cell Signaling Technology, Inc.; 1:1,000)] were incubated overnight. A biotinylated secondary antibody, diluted 1:200 in streptavidin biotinylated horseradish peroxidase for 45 min at RT (Cytiva), was added. Afterwards, 3-amino-9-ethylcarbazole (AEC; ScyTek Laboratories, Inc.) was used as a substrate. All washing procedures were performed in PBS. Slides were counterstained with hematoxylin for 5 min at RT. Sections incubated without the primary antibody served as negative controls and additional controls were performed with the secondary antibody only (data not shown). Samples were imaged using Zeiss Axio Observer Z1 with AxioCam 505 color and analysed with Zen-software version 2.3 (Carl Zeiss AG).

Ex vivo treatment of HNSCC vital tissue cultures. Fresh tissue HNSCC samples (n=4; 1 from the oropharynx, 1 from the oral cavity, 1 from the hypopharynx and 1 from the larynx; Table II) were procured immediately after surgical resection at the Department of Otorhinolaryngology, Head and Neck Surgery, Mannheim University Hospital, Germany. All four donors were male. The mean age was 56.5 years (±1.73 years). Recruitment took place between February 2025 and June 2025. Informed consent was obtained from all subjects involved in the study after the review of the local ethics board (ethic vote 2020-558N). The consent forms provided clear information on the study's purpose, procedures, risks, benefits and the right to withdraw at any time and were presented tailored to the participants' comprehension level. Patients were informed by the principal investigator of the study and consented orally and in written after having the opportunity to ask questions and address concerns. Patients were to be included in the study if they had been diagnosed with HNSCC and have undergone treatment at the Department of Otorhinolaryngology, Head and Neck Surgery, University Hospital Mannheim. Sufficient formalin-fixed paraffin-embedded (FFPE) tumor material had to be available for the planned analyses. Patients were to be excluded from the study if they have a pre-existing mental illness that might interfere with study participation, a history of a previous HNSCC diagnosis, or another active malignant disease at the time of inclusion. Patients with medical conditions associated with an increased risk of bleeding or impaired wound healing were also excluded. Further exclusion criteria include being under the age of 18, not being fully capable of giving informed consent, or testing positive for HIV, HBV, or HCV. Table II gives characteristics of *ex vivo* specimens.

Specimens were transported to the laboratory in transport media (Dulbecco's modified Eagle's medium, supplemented with Primocin) within 30 min after resection. Fresh tissue was sectioned with a scalpel to fragments of 2-3 mm^2 under sterile conditions. For *ex vivo* analysis of tumor response to fractionated IR, tumor sections were maintained in twelve-well plates with inserts (ThinCert; Greiner Bio One Ltd.) in Dulbecco's modified Eagle's medium, supplemented with 10% fetal bovine serum and antibiotics (penicillin 100 U/ml and streptomycin 100 μg/ml). After five days in culture, samples were irradiated on three consecutive days with a daily dose of 2 Gy. Mock-treated samples served as controls. According to the cell line experiments, a linear accelerator with 6 megavolts (MV) photon energy (Elekta Synergy AB) and PMMA plates as water and tissue equivalents, respectively, were employed.

Previously, the total dose and time scheme of 3x2 Gy applied on days 6-8 had been evaluated by dose and time row experiments to achieve an optimal IR effect without overdosing the tissue samples. Fractionated IR instead of a single

dose was chosen to adapt the experimental setting to the norm fractionation scheme applied in HNSCC patients as closely as possible (32,34). The medium was changed every second day. The samples were harvested on day 10 to be evaluated for histopathological and immunohistochemical features (34,35).

Morphological and immunohistochemical evaluation of ex vivo HNSCC cultures. Ex vivo cultivated tissue was FFPE. From these FFPE tissue blocks, 0.5 μM sections were cut and deparaffinized. Hematoxylin and eosin staining, a routine histological technique to visualize tissue morphology was performed (Eosin 10 min, hematoxylin 5 min, at RT). According to the immunohistochemistry protocol used in cell lines, staining was performed analogously with adaptation of the concentrations of antibodies as follows: [Phospho-p44/42 MAPK (Erk1/2; Thr202/Tyr204); cat. no. 9101; Cell Signaling Technology, Inc.; 1:100; t(total) ERK1/2 p44/42 MAPK (ERK1/2); cat. no. 9102; Cell Signaling Technology, Inc.; 1:100; PD-L1; cat. no. 13684; Cell Signaling Technology, Inc.; 1:200, p21 Waf1/Cip1 (12D1) Rabbit mAb cat. no. 2947 Cell Signaling Technology, Inc.; 1:100, phospho-Histone H2A.X (Ser139; 20E3) Rabbit mAb cat. no. 9718, Cell Signaling Technology, Inc.; 1:200]. Incubation with the primary antibodies was at 4˚C overnight.

Quantification of IHC results in cell and tissue cultures. The intensity of IHC staining was determined using the immunoreactive score (IRS) proposed by Remmele and Stegner (36) with slight modifications as follows.

Staining intensity x percentage of positive cells=IRS.

The percentage of immunoreactive tumor cells was rated as follows: No staining=0; less than 10% positive cells=1; 10-50% positive cells=2; 51-80% positive cells=3; greater than 80% positive cells=4. The intensity of staining was evaluated as follows: no color reaction=0; weak/mild color reaction=1; moderate =2; strong/intense color reaction=3. The expression score was obtained by multiplying the percentage of immunoreactive tumor cells by the staining intensity. The score was determined by three independent observers and the mean value was calculated. Shapiro-Wilk-Test was performed with the null hypothesis of normal distribution of the data. Since most p-values were significant a Gaussian distribution was not presumed and statistical significance was calculated using Mann Whitney U test.

Statistical analysis. Results were graphed and analyzed using GraphPad Prism software (version 9.4.1; Dotmatics). Data are presented as means (bars) with standard error of the mean (whiskers) from three independent experiments.

A Shapiro-Wilk test was conducted to assess the normality of the data. Since most P-values were significant, the present study did not assume a Gaussian distribution.

For SA-ß-Gal staining, a Mann-Whitney U test was performed. The null hypothesis stated that there was no difference in positive SA-ß-Gal staining between IR cells and controls.

The results of both *ex vivo* and *in vitro* experiments were also analyzed statistically. Immunoreactivity scores assigned by three independent observers were compared using the Mann-Whitney U test. The null hypothesis stated that there was no difference in scoring between treated cells and mock-treated controls. $P<0.05$ was considered to indicate a statistically significant difference.

Results

Morphologic alterations of the nuclei. Multiple publications describe morphologic alterations, such as enlarged cell volume and nuclei, irregularly shaped nuclei and cytoplasmic vacuoles as characteristic features of senescent cells (37-39). After fractionated IR, the present study found a subpopulation of tumor cells with enlarged nuclei in all three HNSCC cell lines (Fig. 1A). Other morphologic alterations, such as enlarged cell volume, irregularly shaped nuclei and cytoplasmic vacuoles as characteristic features of senescence, were also visible. The altered morphology was clearly recognizable across all cell lines. There was a small number of cells with this phenotype in untreated cells, which distinctly increased in response to fractionated IR.

Evidence for senescence induction by SA-ß-Gal staining. To confirm a potential induction of senescence by fractionated IR, SA-ß-Gal staining was performed.

SA-ß-Gal staining is a widely used histochemical assay to detect cellular senescence. It identifies senescent cells by measuring ß-galactosidase enzyme activity at pH 6.0, a characteristic feature of senescent cells. The assay involves staining cells or tissue samples with X-gal, a substrate that produces a blue color when cleaved by SA-ß-Gal.

An increase in SA-ß-Gal was observed after irradiation in all cell lines, which was most distinct in UMSCC-14C cells. In UM-SCC 22B the changes where statistically significant (P=0.0286; Fig. 1A; for quantification see Fig. 1B).

Effect of fractioned IR on proliferation of senescence marker p21. To further confirm senescence induction, IHC staining of the senescence marker p21 was performed. As seen in Fig. 2, there was a slight increase in p21 protein expression in UM-SCC-11B and UM-SCC-22B as well as a marked increase in UM-SCC-14C compared with mock-treated controls (Fig. 2A and B).

Effect of fractioned IR on proliferation of γH2AX. There was a visible increase in positive staining of γH2AX indicating post-radiogenic DNA double strand breaks in all three cell lines, but due to the small sample size the results of the statistical evaluation were non-significant (11B P=0.059; 14C P=0.48; 22B P=0.3; Fig. 2A and B).

Fractionated IR modulates PD-L1 surface expression. Unlike in previous studies where cells and tissue samples were treated with a single irradiation dose and immediately analyzed post IR, the present study was interested in examining also mid- and long-term adjustment mechanisms to a fractionated protocol (4x2 Gy) according to the norm fractionation scheme applied to HNSCC patients. All three cell lines displayed a strong induction of PD-L1 which was most distinct in cells from the UM-SCC-22B cell line (Fig. 2A and B).

Effect of fractionated IR on MAPK ERK signaling. UM-SCC-22B cells showed a strong induction of activated ERK1/2, similar to the PD-L1 expression pattern. There was a minor induction in pERK1/2 in UM-SCC-14C, while no

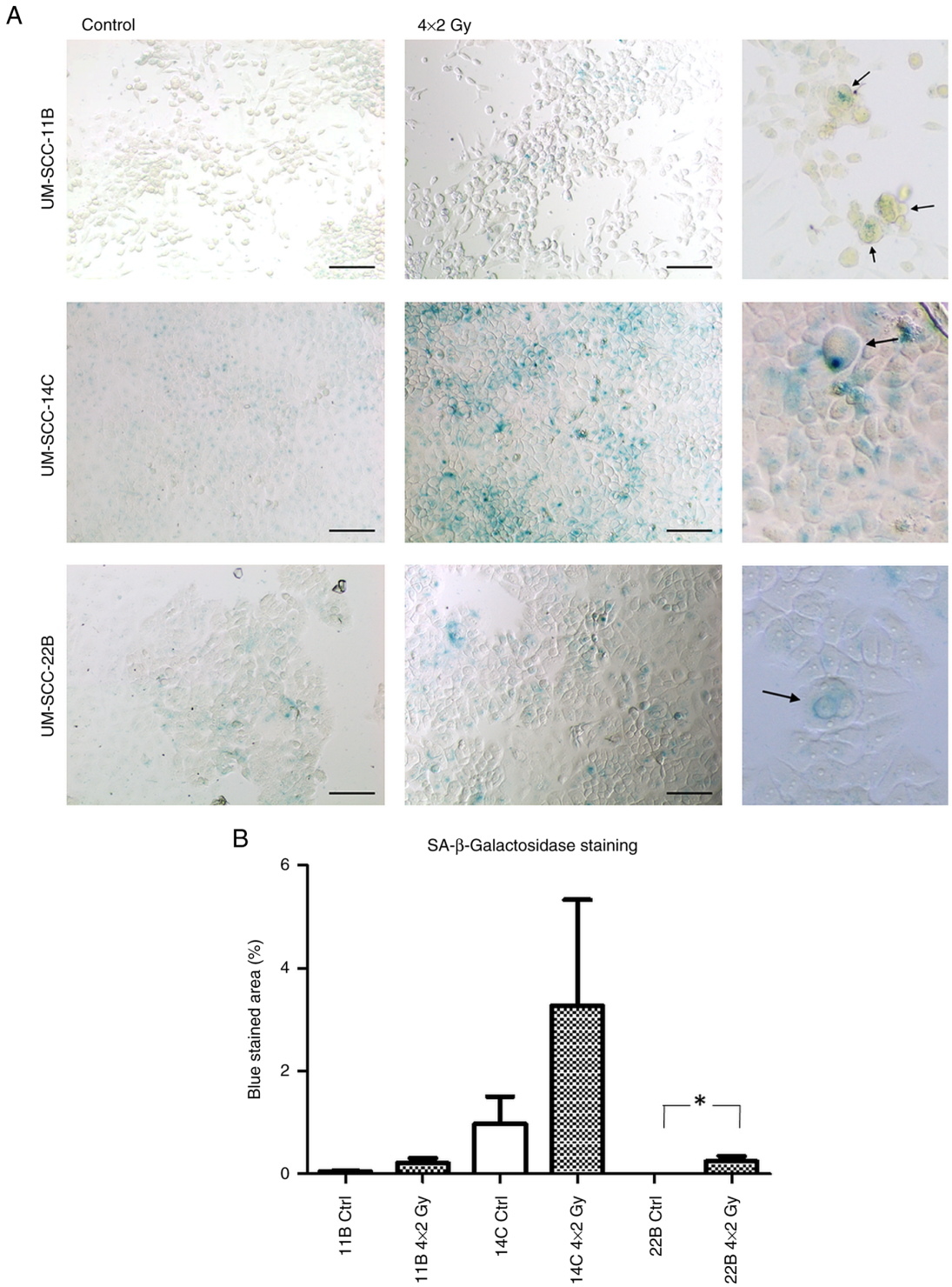

Figure 1. Irradiation-induced senescence in HNSCC cell lines detected by SA-β-Gal staining. (A) Irradiation-induced senescence in HNSCC cell lines UM-SCC-11B, UM-SCC-14C and UM-SCC-22B. Left panel: Mock-treated controls; middle panel: irradiated cells (4x2 Gy); right panel: section enlargement of irradiated batch. SA-β-Gal staining reveals senescent cells (green-blue signal). Arrows (right panel) indicate morphologic cellular features typical for senescence (enlarged and flattened cells) (scale bar, 100 μm). (B) Quantification of postradiogenic senescence induction in HNSCC cell lines. The y-axis displays SA-β-Gal positive cells as a percentage of the total number of cells (median + SEM). Experiments were performed in triplicates. For significance calculation, Mann Whitney U test was applied. *P=0.0286. HNSCC, head and neck squamous cell carcinoma; SA-β-Gal, senescence-associated β-galactosidase.

modifications in pERK1/2 protein expression were detected in UM-SCC-11B compared with mock-treated controls (Fig. 2A and B).

Validation of senescence-associated markers in a 3D ex vivo HNSCC tissue culture model. In order to verify the findings of cellular response to fractionated IR observed in the cell lines, the expression of senescence-associated markers was validated in human HNSCC tumor tissue. This explant model offers the advantage of taking the composition of the individual patient's tumor and a potential impact of the TME into account, which is not depicted in 2D cell culture model.

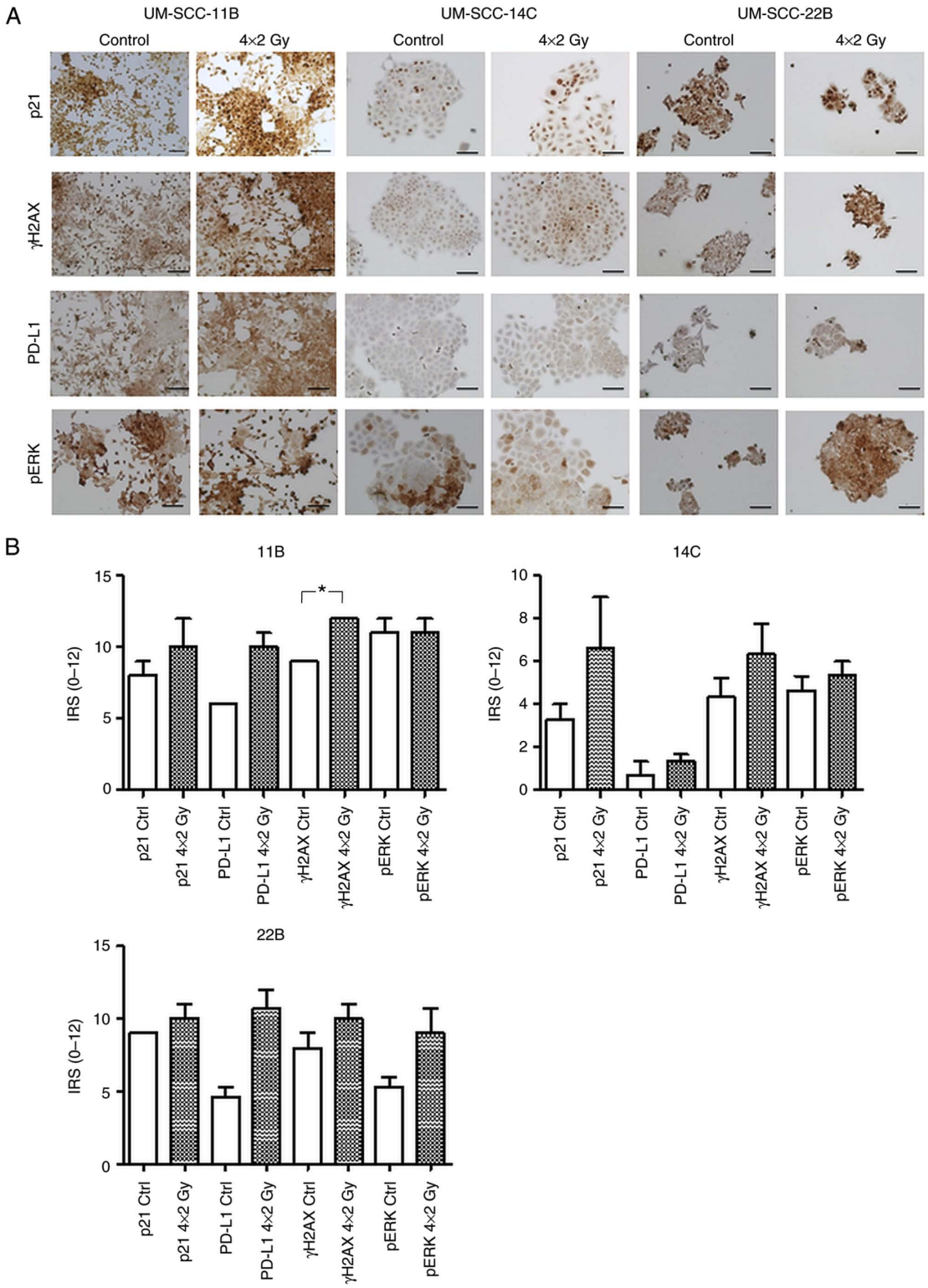

Figure 2. Differential expression and quantification of p21, pERK1/2, PD-L1 and γH2AX in HNSCC cell lines following fractionated IR. (A) Expression of p21, pERK1/2, PD-L1 and γH2AX in HNSCC cell lines UM-SCC-11B, UM-SCC-14C and UM-SCC-22B post IR. IHC staining of p21, γH2AX, PD-L1 and pERK1/2 after fractionated IR (4x2 Gy) compared with mock-treated controls displayed differential modulations of target proteins (representative images shown). (B) Quantification of IHC results. The IRS was obtained by visual examination. Results were quantified using the IRS modified according to Remmele and Stegner (36). The mean ± SD value was calculated. Statistical significance ($^{*}P<0.05$) was assessed using Mann Whitney U test. p, phosphorylated; PD-L1, programmed death-ligand 1; γH2AX, histone H2AX; HNSCC, head and neck squamous cell carcinoma; IR, ionizing radiation; IHC, immunohistochemistry; IRS, immunoreactive score. Scale bar=100 μm.

One specimen each from the typical anatomical HNSCC sites (oral cavity, oropharynx, hypopharynx, larynx) was included.

A statistically significant increase in p21 expression post IR was observed in all four specimens indicating that

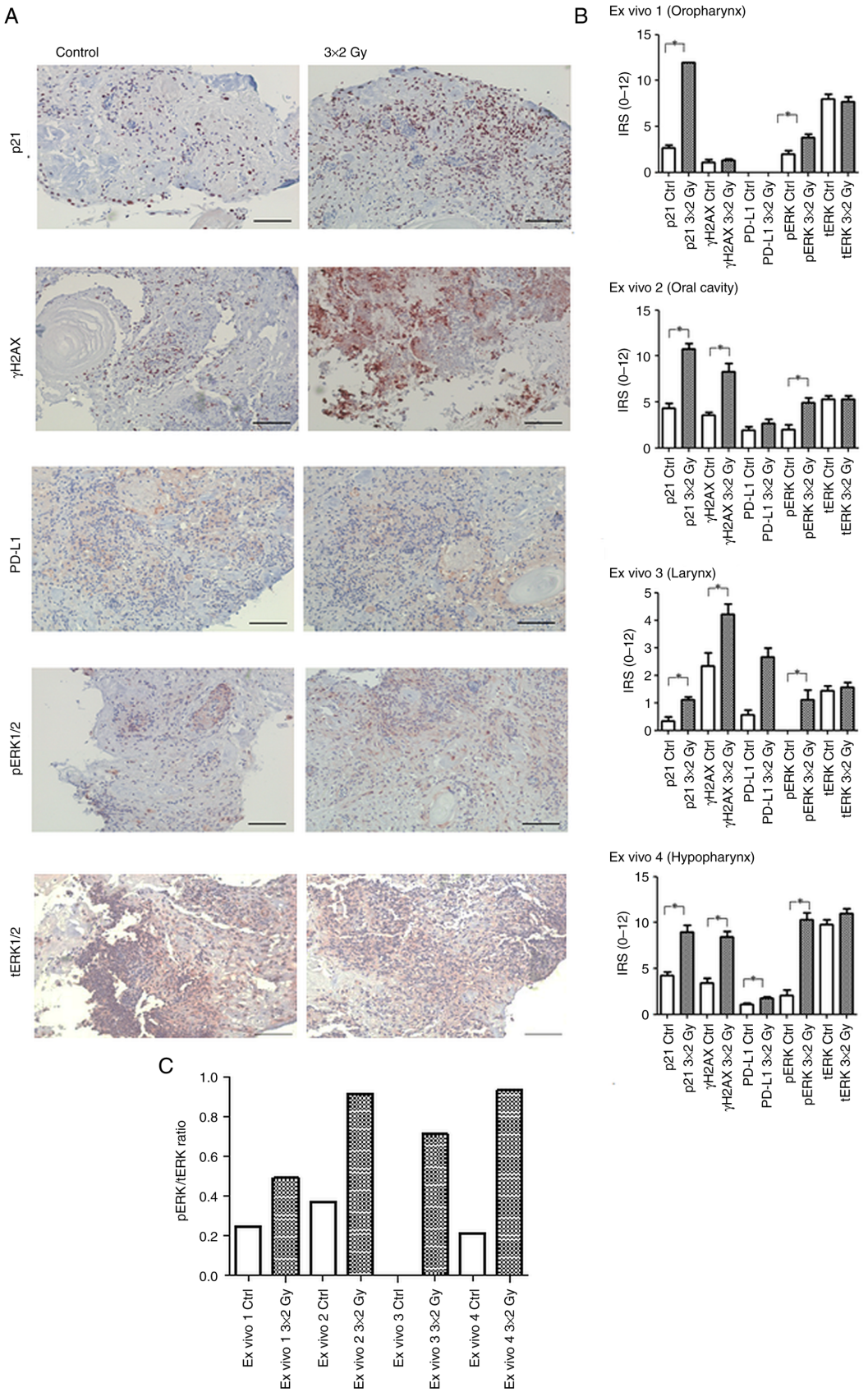

Figure 3. Expression and quantification of p21, γH2AX, PD-L1, and ERK1/2 in irradiated 3D *ex vivo* HNSCC tissue. (A) IHC staining of p21, γH2AX, PD-L1, pERK1/2 and tERK1/2 in irradiated 3D *ex vivo* HNSCC tissue cultures. Expression patterns in an *ex vivo* human HNSCC tissue culture model. Simultaneous increase of PD-L1 and p21 after fractionated IR in the IHC, compared with mock-treated controls (representative images shown; scale bar, 100 μm). (B) Quantification of IHC results. The IRS was obtained by visual examination. Results were quantified using the IRS modified according to Remmele and Stegner (36) as performed for the *in vitro* data. The mean ± SD was calculated. Statistical significance ($^*P<0.05$) was assessed using Mann Whitney U tests. (C) pERK1/2 to tERK1/2 ratio in *ex vivo* samples following radiation treatment. Bar graph showing the pERK1/2/ERK1/2 ratio in *ex vivo* 1-4. IHC, immunohistochemistry; γH2AX, histone H2AX; PD-L1, programmed death-ligand 1; p, phosphorylated; HNSCC, head and neck squamous cell carcinoma; IR, ionizing radiation; IHC, immunohistochemistry; IRS, immunoreactive score. Scale bar=100 μm.

radiotherapy affects senescence regulation (EV1 P=0.0001, EV2 P=0.003, EV 3 P=0.004, EV 4 P=0.0005). Accordingly, there was a parallel raise in γH2AX as additional senescence marker in all samples. The difference reached significance in oral cavity, larynx and hypopharynx samples (EV2 P=0.0002, EV3 P=0.0137, EV 4 P=0.0004).

As expected, the 3D model enabled confirmation of the 2D results regarding a postradiogenic upregulation of PD-L1 and pERK1/2. Except the oropharyngeal specimen, which did not express any PD-L1 at baseline and after treatment, PD-L1 levels were significantly enhanced after IR in the hypopharyngeal tissue (P=0.0066) while there was a minor increase in *ex vivo* specimens derived from the larynx and the oral cavity. pERK1/2 was activated in all four *ex vivo* samples reaching significance in all cases (EV1: P=0.011; EV2: 0.0039; EV3: 0.0052; EV4: 0,0004). tERK1/2 expression appeared stable after fractionated IR in all specimens (Fig. 3A and B).

Discussion

The present study described the expression of senescence-associated molecules γH2AX, SA-β-Gal and p21, alongside morphological criteria for detecting senescence in HNSCC cell lines and viable HNSCC human tissue samples. The findings demonstrated that these features are associated with irradiation-induced induction of PD-L1 along with activation of the MAPK ERK survival pathway.

In HNSCC patients, norm-fractionated radiotherapy alone is most commonly administered at a dose of 1.6-2.0 Gy per fraction per day, five days a week, over a period of 6-7 weeks (40). Therefore, the present study established an experimental regimen using single daily fractions of 2 Gy, based on our previous demonstration that these doses are sufficient to produce an effect (32,34). It is well established that standard oncological treatments, such as radiochemotherapy (RCT), induce senescence in solid tumors (40-42). Additionally, senescent cells are known to contribute to certain chemotherapy-related side effects (43,44). The senescent phenotype is characterized by irreversible growth arrest while maintaining viability and metabolic activity. Key features of this phenotype include distinct cellular morphology (enlarged and flattened cells), increased expression of p53 and p21, markers of DNA double-strand breaks (DSBs) and the presence of SA-ß-Gal, along with an elevated number of γH2AX foci, one of the most sensitive markers of DSBs (45-48).

Standard oncological treatment such as RCT induces senescence in solid tumors (41-43) Additionally, senescent cells are known to cause certain chemotherapy-related side effects (38,44). The senescent phenotype is featured by irreversible growth arrest while maintaining viability and metabolic activity. This phenotype includes a distinct cellular morphology (enlarged and flattened cells), increased expression of p53, p21, markers of DNA DSBs and the presence of SA-ß-Gal as well as an increased number of γH2AX foci, the most sensitive marker of DSBs (39,45-47). Senescence has been described as a double-edged sword exhibiting both tumor suppressive and promoting properties (48-51). While therapy-induced senescence can contribute to metastasis, recurrence and adverse reactions to cancer treatment (52), current anti-cancer strategies provide an ideal foundation for TME-associated damage responses, which result in the promotion of senescence as a resistance mechanism (53): It is well documented that senescent cells within the TME contribute to tumor progression, metastasis and therapy resistance (54). Cellular senescence is increasingly recognized as a patients' response to various anticancer therapies (55) and is probably associated with poor treatment response in different cancer entities (56-59).

As one of the most prominent markers of senescence, p21 has been described to harbor either tumor suppressor activity or tumor-promoting properties (60). In the p21 analyses, the present study detected an increased postradiogenic nuclear p21 expression in HNSCC tumor cell lines and *ex vivo* cultures, accompanied by an increase in ß Gal positive cells and γH2AX protein levels, compared with control, indicating that IR might trigger senescence in HNSCC cells which could induce resistance to this fundamental treatment pillar.

In parallel, the MAPK signaling pathway plays an important role in oncogene-induced senescence (61,62). MEK and subsequently ERK1/2, so-called gerogens, are capable of arresting the cell cycle via p53, p21 and p16 (63). Patel *et al* (64) recently showed that continued MAPK/ERK activation in oncogene-induced senescent cells offers a potential escape route after ~1 month leading to c-MYC dependent reactivation of telomerase. This reinforces the role of MAPK/ERK in the formation of resistance based on senescent cells. While there are various 3D models of ERK-induced senescence, so far none have been detected specifically for head and neck cancer (65).

Woo *et al* (66) describe that that inhibition of MEK and PI3K signaling pathways increases the sensitivity of HNSCC cells to radiotherapy by enhancing therapy-induced senescence. However, this study was only conducted in a 2D cell culture approach, which does not reflect tumor-TME interactions. Indeed, a rationale for including the tumor-TME-interrelations when investigating senescence is provided by studies showing that the epithelial to mesenchymal transition phenotype is resistant to radiochemotherapy (67) and that interactions with the TME can influence the tumor's sensitivity against treatment (68). A improved understanding of this mechanism is of great interest as there is evidence for radioresistance already in quiescent cells in HNSCC cell lines (69). This aggressive phenotype could be further promoted by coexisting senescent cells (70,71) leading to an undesirable outcome that must not be underestimated.

Similarly, the immune checkpoint molecule PD-L1, the ligand for PD-1 on immune cells, which drives immune cell inactivation, is associated with cellular senescence. In line with the present data, Onorati *et al* (25) report that senescent cells upregulate PD-L1. This induction of PD-L1 in senescence is shown to depend on the proinflammatory program. The clinical benefit of PD-1 inhibitors is restricted by immunosuppressive properties of the TME (72-74) and the insufficient reactivation of antitumor immunity by the drug alone (75). There have been considerations as to whether responses to CPI are linked to cellular senescence as CPI treatment has been observed to increase the presence of senescent T cells (76). These findings on a potential link between senescence and CPI response justify the employment of 2D and 3D HNSCC models as performed in the

present study as only <20% of HNSCC patients respond to CPI monotherapy (77). So more elucidation of factors contributing to CPI sensitivity are clearly needed. For other tumor entities such as breast cancer this issue has already been addressed. Si *et al* (4) observed that blockade of PD-L1 and STAT3 could prevent tumor-associated regulatory T cell-induced senescence in dendritic cells. Although that study focuses on breast cancer, the results may also be relevant for head and neck cancer, as similar mechanisms of immunomodulation may be involved.

The present study included cell lines and tissue samples from different localities in the head and neck region to illustrate diversity in tumoral behavior, which is known to be associated with varying response to cancer treatment and found comparable results. This observation is particularly notable because it has variously been shown that differences in survival and molecular biology exist between HNSCC anatomical sites and TME of these sites may guide immune and radiation therapies (78). However, this observation is provisional, as the present sample size was small, which must be considered as a limitation of the study. The results can be considered more of a pilot project but are worth testing in a larger cohort. In terms of clinical applicability, it could be of relevance that recent data show senolytic agents such as B-cell lymphoma-x large inhibitor ABT-263 (Navitoclax) in combination with cisplatin probably being useful for eliminating residual senescent tumor cells after chemotherapy and thereby potentially delay disease recurrence in head and neck cancer patients (79).

Hence, it is expected, based on these and previous data, that the *ex vivo* model is a useful tool to provide a platform for sensitivity testing of novel combination therapies, such as cisplatin and senolytics, as part of a personalized treatment approach.

The prognostic effect of therapy-induced senescence remains incomplete. Previously we demonstrated tumor cell-mediated regulation of PD-L1 upon platinum-based CRT in HNSCC and their exosomes (32). The present study aimed to define whether there is a correlation between postradiogenic induction of senescence, ERK1/2 signaling and PD-L1 expression. The data provided evidence that fractionated IR generated a subpopulation of HNSCC tumor cells exhibiting senescence-associated cellular changes and increased expression of pERK1/2 and PD-L1. The results suggested a link between survival signaling, radiation-induced checkpoint activation and the emergence of senescence in HNSCC. Additionally, the *ex vivo* 3D tissue model has proved to be a valuable tool for validation and complementing *in vitro* data, offering insights into tumor-TME correlations. In the future, further analyses, particularly in larger cohorts, are required to better elucidate the clinical relevance and significance of therapy-induced senescence in the treatment of cancer patients.

Acknowledgements

The authors gratefully acknowledge the excellent technical support of Ms. Petra Prohaska, Scientific Laboratory at Department of Otorhinolaryngology, Head and Neck Surgery, University Hospital Mannheim, Medical Faculty Mannheim of Heidelberg University, Mannheim, Germany.

Funding

The present study was substantially supported by the Program for the Promotion of Equality and Careers of Female Physicians and Scientists at the University Medical Center Mannheim (to AA).

Availability of data and materials

The data generated in the present study are included in the figures and/or tables of this article.

Authors' contributions

LB and AA were responsible for data curation and formal analysis. Funding acquisition was by AA and ES. FJ, JF and AL made substantial contributions to the acquisition, analysis, and interpretation of data for the work. Supervision was by JK, NR and CS. Visualization was by AA, LB and ES. Writing the original draft was by LB and AA. Writing, reviewing and editing was by LB, AA, CS, JK and NR. LB, AA, and JK confirm the authenticity of all the raw data. All authors have read and approved the final manuscript.

Ethics approval and consent to participate

The study was conducted according to the guidelines of the Declaration of Helsinki and approved by the Institutional Review Board (or Ethics Committee) of Heidelberg University, Medical Faculty Mannheim (protocol code 2020-558N, date of approval 4 Jun 2020). Informed consent was obtained from all subjects involved in the study.

Patient consent for publication

Not applicable.

Competing interests

The authors declare that they have no competing interests.

References

1. Herranz N and Gil J: Mechanisms and functions of cellular senescence. J Clin Invest 128: 1238-1246, 2018.
2. Kim HS, Song MC, Kwak IH, Park TJ and Lim IK: Constitutive induction of p-Erk1/2 accompanied by reduced activities of protein phosphatases 1 and 2A and MKP3 due to reactive oxygen species during cellular senescence. J Biol Chem 278: 37497-37510, 2003.
3. White RR and Vijg J: Do DNA double-strand breaks drive aging? Mol Cell 63: 729-738, 2016.
4. Si F, Liu X, Tao Y, Zhang Y, Ma F, Hsueh EC, Puram SV and Peng G: Blocking senescence and tolerogenic function of dendritic cells induced by γδ Treg cells enhances tumor-specific immunity for cancer immunotherapy. J Immunother Cancer 12: e008219, 2024.
5. Ruhland MK and Alspach E: Senescence and immunoregulation in the tumor microenvironment. Front Cell Dev Biol 9: 754069, 2021.
6. Toso A, Revandkar A, Di Mitri D, Guccini I, Proietti M, Sarti M, Pinton S, Zhang J, Kalathur M, Civenni G, *et al*: Enhancing chemotherapy efficacy in Pten-deficient prostate tumors by activating the senescence-associated antitumor immunity. Cell Rep 9: 75-89, 2014.

7. Wang J, Zhou CC, Sun HC, Li Q, Hu JD, Jiang T and Zhou S: Identification of several senescence-associated genes signature in head and neck squamous cell carcinoma. J Clin Lab Anal 36: e24555, 2022.
8. Ostrowska K, Niewinski P, Piotrowski I, Ostapowicz J, Koczot S, Suchorska WM, Golusiński P, Masternak MM and Golusiński W: Senescence in head and neck squamous cell carcinoma: relationship between senescence-associated secretory phenotype (SASP) mRNA expression level and clinicopathological features. Clin Transl Oncol 26: 1022-1032, 2024.
9. Schoetz U, Klein D, Hess J, Shnayien S, Spoerl S, Orth M, Mutlu S, Hennel R, Sieber A, Ganswindt U, *et al*: Early senescence and production of senescence-associated cytokines are major determinants of radioresistance in head-and-neck squamous cell carcinoma. Cell Death Dis 12: 1162, 2021.
10. Lee YC, Nam Y, Kim M, Kim SI, Lee JW, Eun YG and Kim D: Prognostic significance of senescence-related tumor microenvironment genes in head and neck squamous cell carcinoma. Aging (Albany NY) 16: 985-1001, 2023.
11. McCubrey JA, Steelman LS, Chappell WH, Abrams SL, Wong EW, Chang F, Lehmann B, Terrian DM, Milella M, Tafuri A, *et al*: Roles of the Raf/MEK/ERK pathway in cell growth, malignant transformation and drug resistance. Biochim Biophys Acta 1773: 1263-1284, 2007.
12. Golding SE, Morgan RN, Adams BR, Hawkins AJ, Povirk LF and Valerie K: Pro-survival AKT and ERK signaling from EGFR and mutant EGFRvIII enhances DNA double-strand break repair in human glioma cells. Cancer Biol Ther 8: 730-738, 2009.
13. Hein AL, Ouellette MM and Yan Y: Radiation-induced signaling pathways that promote cancer cell survival (review). Int J Oncol 45: 1813-1819, 2014.
14. Chung EJ, Brown AP, Asano H, Mandler M, Burgan WE, Carter D, Camphausen K and Citrin D: In vitro and in vivo radiosensitization with AZD6244 (ARRY-142886), an inhibitor of mitogen-activated protein kinase/extracellular signal-regulated kinase 1/2 kinase. Clin Cancer Res 15: 3050-3057, 2009.
15. Leiker AJ, DeGraff W, Choudhuri R, Sowers AL, Thetford A, Cook JA, Van Waes C and Mitchell JB: Radiation enhancement of head and neck squamous cell carcinoma by the Dual PI3K/mTOR Inhibitor PF-05212384. Clin Cancer Res 21: 2792-2801, 2015.
16. Affolter A, Drigotas M, Fruth K, Schmidtmann I, Brochhausen C, Mann WJ and Brieger J: Increased radioresistance via G12S K-Ras by compensatory upregulation of MAPK and PI3K pathways in epithelial cancer. Head Neck 35: 220-228, 2013.
17. Affolter A, Fruth K, Brochhausen C, Schmidtmann I, Mann WJ and Brieger J: Activation of mitogen-activated protein kinase extracellular signal-related kinase in head and neck squamous cell carcinomas after irradiation as part of a rescue mechanism. Head Neck 33: 1448-1457, 2011.
18. Affolter A and Hess J: Preclinical models in head and neck tumors: Evaluation of cellular and molecular resistance mechanisms in the tumor microenvironment. HNO 64: 860-869, 2016 (In German).
19. Affolter A, Samosny G, Heimes AS, Schneider J, Weichert W, Stenzinger A, Sommer K, Jensen A, Mayer A, Brenner W, *et al*: Multikinase inhibitors sorafenib and sunitinib as radiosensitizers in head and neck cancer cell lines. Head Neck 39: 623-632, 2017.
20. Perri F, Pacelli R, Della Vittoria Scarpati G, Cella L, Giuliano M, Caponigro F and Pepe S: Radioresistance in head and neck squamous cell carcinoma: Biological bases and therapeutic implications. Head Neck 37: 763-770, 2015.
21. Sharon S and Bell RB: Immunotherapy in head and neck squamous cell carcinoma: A narrative review. Front Oral Maxillofac Med 4: 28, 2022.
22. Chen Z, Wong PY, Ng CWK, Lan L, Fung S, Li JW, Cai L, Lei P, Mou Q, Wong SH, *et al*: The intersection between oral microbiota, host gene methylation and patient outcomes in head and neck squamous cell carcinoma. Cancers (Basel) 12: 3425, 2020.
23. Affolter A, Kern J, Bieback K, Scherl C, Rotter N and Lammert A: Biomarkers and 3D models predicting response to immune checkpoint blockade in head and neck cancer (Review). Int J Oncol 61: 88, 2022.
24. Wang TW, Johmura Y, Suzuki N, Omori S, Migita T, Yamaguchi K, Hatakeyama S, Yamazaki S, Shimizu E, Imoto S, *et al*: Blocking PD-L1-PD-1 improves senescence surveillance and ageing phenotypes. Nature 611: 358-364, 2022.
25. Onorati A, Havas AP, Lin B, Rajagopal J, Sen P, Adams PD and Dou Z: Upregulation of PD-L1 in Senescence and Aging. Mol Cell Biol 42: e0017122, 2022.
26. Brenner E, Schörg BF, Ahmetlić F, Wieder T, Hilke FJ, Simon N, Schroeder C, Demidov G, Riedel T, Fehrenbacher B, *et al*: Cancer immune control needs senescence induction by interferon-dependent cell cycle regulator pathways in tumours. Nat Commun 11: 1335, 2020.
27. Chen Z, Hu K, Feng L, Su R, Lai N, Yang Z and Kang S: Senescent cells re-engineered to express soluble programmed death receptor-1 for inhibiting programmed death receptor-1/programmed death ligand-1 as a vaccination approach against breast cancer. Cancer Sci 109: 1753-1763, 2018.
28. Zhang J, Bu X, Wang H, Zhu Y, Geng Y, Nihira NT, Tan Y, Ci Y, Wu F, Dai X, *et al*: Cyclin D-CDK4 kinase destabilizes PD-L1 via cullin 3-SPOP to control cancer immune surveillance. Nature 553: 91-95, 2018.
29. Lee JJ, Kim SY, Kim SH, Choi S, Lee B and Shin JS: STING mediates nuclear PD-L1 targeting-induced senescence in cancer cells. Cell Death Dis 13: 791, 2022.
30. Moreira A, Gross S, Kirchberger MC, Erdmann M, Schuler G and Heinzerling L: Senescence markers: Predictive for response to checkpoint inhibitors. Int J Cancer 144: 1147-1150, 2019.
31. Abdel-Naby R, Wang K, Song D, Bozentka J, LaFonte M, Ou P, Stanek A, Mueller C, Alfonso A and Huan C: Extracellular Signal-Regulated Kinase (ERK)-dependent p21 (WAF1/Cip1) Expression Is Associated with Gemcitabine Resistance in Pancreatic Cancer Cells. J Am Coll Surg 219: S27, 2014.
32. Affolter A, Liebel K, Tengler L, Seiz E, Tiedtke M, Azhakesan A, Schütz J, Theodoraki MN, Kern J, Ruder AM, *et al*: Modulation of PD-L1 expression by standard therapy in head and neck cancer cell lines and exosomes. Int J Oncol 63: 102, 2023.
33. Welters MJ, Fichtinger-Schepman AM, Baan RA, Hermsen MA, van der Vijgh WJ, Cloos J and Braakhuis BJ: Relationship between the parameters cellular differentiation, doubling time and platinum accumulation and cisplatin sensitivity in a panel of head and neck cancer cell lines. Int J Cancer 71: 410-415, 1997.
34. Engelmann L, Thierauf J, Koerich Laureano N, Stark HJ, Prigge ES, Horn D, Freier K, Grabe N, Rong C, Federspil P, *et al*: Organotypic co-cultures as a novel 3D model for head and neck squamous cell carcinoma. Cancers (Basel) 12: 2330, 2020.
35. Affolter A, Muller MF, Sommer K, Stenzinger A, Zaoui K, Lorenz K, Wolf T, Sharma S, Wolf J, Perner S, *et al*: Targeting irradiation-induced mitogen-activated protein kinase activation in vitro and in an ex vivo model for human head and neck cancer. Head Neck 38 (Suppl 1): E2049-E2061, 2016.
36. Remmele W and Stegner HE: Recommendation for uniform definition of an immunoreactive score (IRS) for immunohistochemical estrogen receptor detection (ER-ICA) in breast cancer tissue. Pathologe 8: 138-140, 1987 (In German).
37. Muñoz-Espín D and Serrano M: Cellular senescence: From physiology to pathology. Nat Rev Mol Cell Biol 15: 482-496, 2014.
38. Demaria M: Senescent cells: New target for an old treatment? Mol Cell Oncol 4: e1299666, 2017.
39. Bernadotte A, Mikhelson VM and Spivak IM: Markers of cellular senescence. Telomere shortening as a marker of cellular senescence. Aging (Albany NY) 8: 3-11, 2016.
40. Matuschek C, Haussmann J, Bölke E, Gripp S, Schuler PJ, Tamaskovics B, Gerber PA, Djiepmo-Njanang FJ, Kammers K, Plettenberg C, *et al*: Accelerated vs. conventionally fractionated adjuvant radiotherapy in high-risk head and neck cancer: A meta-analysis. Radiat Oncol 13: 195, 2018.
41. Qin S, Schulte BA and Wang GY: Role of senescence induction in cancer treatment. World J Clin Oncol 9: 180-187, 2018.
42. Milanovic M, Fan DNY, Belenki D, Däbritz JHM, Zhao Z, Yu Y, Dörr JR, Dimitrova L, Lenze D, Monteiro Barbosa IA, *et al*: Senescence-associated reprogramming promotes cancer stemness. Nature 553: 96-100, 2018.
43. Nicolas AM, Pesic M, Engel E, Ziegler PK, Diefenhardt M, Kennel KB, Buettner F, Conche C, Petrocelli V, Elwakeel E, *et al*: Inflammatory fibroblasts mediate resistance to neoadjuvant therapy in rectal cancer. Cancer Cell 40: 168-184.e13, 2022.
44. Demaria M, O'Leary MN, Chang J, Shao L, Liu S, Alimirah F, Koenig K, Le C, Mitin N, Deal AM, *et al*: Cellular senescence promotes adverse effects of chemotherapy and cancer relapse. Cancer Discov 7: 165-176, 2017.
45. Gu L and Kitamura M: Sensitive detection and monitoring of senescence-associated secretory phenotype by SASP-RAP assay. PLoS One 7: e52305, 2012.

46. Redon CE, Nakamura AJ, Sordet O, Dickey JS, Gouliaeva K, Tabb B, Lawrence S, Kinders RJ, Bonner WM and Sedelnikova OA: γ-H2AX detection in peripheral blood lymphocytes, splenocytes, bone marrow, xenografts, and skin. Methods Mol Biol 682: 249-270, 2011.
47. Sedelnikova OA, Horikawa I, Zimonjic DB, Popescu NC, Bonner WM and Barrett JC: Senescing human cells and ageing mice accumulate DNA lesions with unrepairable double-strand breaks. Nat Cell Biol 6: 168-170, 2004.
48. Golomb L, Sagiv A, Pateras IS, Maly A, Krizhanovsky V, Gorgoulis VG, Oren M and Ben-Yehuda A: Age-associated inflammation connects RAS-induced senescence to stem cell dysfunction and epidermal malignancy. Cell Death Differ 22: 1764-1774, 2015.
49. Krtolica A, Parrinello S, Lockett S, Desprez PY and Campisi J: Senescent fibroblasts promote epithelial cell growth and tumorigenesis: A link between cancer and aging. Proc Natl Acad Sci USA 98: 12072-12077, 2001.
50. Halazonetis TD, Gorgoulis VG and Bartek J: An oncogene-induced DNA damage model for cancer development. Science 319: 1352-1355, 2008.
51. Serrano M, Lin AW, McCurrach ME, Beach D and Lowe SW: Oncogenic ras provokes premature cell senescence associated with accumulation of p53 and p16INK4a. Cell 88: 593-602, 1997.
52. Wang B, Kohli J and Demaria M: Senescent cells in cancer therapy: Friends or Foes? Trends Cancer 6: 838-857, 2020.
53. Gordon RR and Nelson PS: Cellular senescence and cancer chemotherapy resistance. Drug Resist Updat 15: 123-131, 2012.
54. D'Ambrosio M and Gil J: Reshaping of the tumor microenvironment by cellular senescence: An opportunity for senotherapies. Dev Cell 58: 1007-1021, 2023.
55. Domen A, Deben C, Verswyvel J, Flieswasser T, Prenen H, Peeters M, Lardon F and Wouters A: Cellular senescence in cancer: Clinical detection and prognostic implications. J Exp Clin Cancer Res 41: 360, 2022.
56. George B, Horn D, Bayo P, Zaoui K, Flechtenmacher C, Grabe N, Plinkert P, Krizhanovsky V and Hess J: Regulation and function of Myb-binding protein 1A (MYBBP1A) in cellular senescence and pathogenesis of head and neck cancer. Cancer Lett 358: 191-199, 2015.
57. Mosieniak G, Sliwinska M, Alster O, Strzeszewska A, Sunderland P, Piechota M, Was H and Sikora E: Polyploidy formation in doxorubicin-treated cancer cells can favor escape from senescence. Neoplasia 17: 882-893, 2015.
58. Wang Q, Wu PC, Dong DZ, Ivanova I, Chu E, Zeliadt S, Vesselle H and Wu DY: Polyploidy road to therapy-induced cellular senescence and escape. Int J Cancer 132: 1505-1515, 2013.
59. Zhai J, Han J, Li C, Lv D, Ma F and Xu B: Tumor senescence leads to poor survival and therapeutic resistance in human breast cancer. Front Oncol 13: 1097513, 2023.
60. Stivala LA, Cazzalini O and Prosperi E: The cyclin-dependent kinase inhibitor p21CDKN1A as a target of anti-cancer drugs. Curr Cancer Drug Targets 12: 85-96, 2012.
61. Xu Y, Li N, Xiang R and Sun P: Emerging roles of the p38 MAPK and PI3K/AKT/mTOR pathways in oncogene-induced senescence. Trends Biochem Sci 39: 268-276, 2014.
62. Anerillas C, Abdelmohsen K and Gorospe M: Regulation of senescence traits by MAPKs. Geroscience 42: 397-408, 2020.
63. Chambard JC, Lefloch R, Pouysségur J and Lenormand P: ERK implication in cell cycle regulation. Biochim Biophys Acta 1773: 1299-1310, 2007.
64. Patel PL, Suram A, Mirani N, Bischof O and Herbig U: Derepression of hTERT gene expression promotes escape from oncogene-induced cellular senescence. Proc Natl Acad Sci USA 113: E5024-E5033, 2016.
65. Schmitt CA, Wang B and Demaria M: Senescence and cancer-role and therapeutic opportunities. Nat Rev Clin Oncol 19: 619-636, 2022.
66. Woo SH, Yang LP, Chuang HC, Fitzgerald A, Lee HY, Pickering C, Myers JN and Skinner HD: Down-regulation of malic enzyme 1 and 2: Sensitizing head and neck squamous cell carcinoma cells to therapy-induced senescence. Head Neck 38 (Suppl 1): E934-E940, 2016.
67. McConkey DJ, Choi W, Marquis L, Martin F, Williams MB, Shah J, Svatek R, Das A, Adam L, Kamat A, *et al*: Role of epithelial-to-mesenchymal transition (EMT) in drug sensitivity and metastasis in bladder cancer. Cancer Metastasis Rev 28: 335-344, 2009.
68. Khalaf K, Hana D, Chou JT, Singh C, Mackiewicz A and Kaczmarek M: Aspects of the tumor microenvironment involved in immune resistance and drug resistance. Front Immunol 12: 656364, 2021.
69. Eckers JC, Kalen AL, Sarsour EH, Tompkins VS, Janz S, Son JM, Doskey CM, Buettner GR and Goswami PC: Forkhead box M1 regulates quiescence-associated radioresistance of human head and neck squamous carcinoma cells. Radiat Res 182: 420-429, 2014.
70. Cahu J, Bustany S and Sola B: Senescence-associated secretory phenotype favors the emergence of cancer stem-like cells. Cell Death Dis 3: e446, 2012.
71. Özcan S, Alessio N, Acar MB, Mert E, Omerli F, Peluso G and Galderisi U: Unbiased analysis of senescence associated secretory phenotype (SASP) to identify common components following different genotoxic stresses. Aging (Albany NY) 8: 1316-1329, 2016.
72. Fares CM, Van Allen EM, Drake CG, Allison JP and Hu-Lieskovan S: Mechanisms of resistance to immune checkpoint blockade: Why does checkpoint inhibitor immunotherapy not work for all patients? Am Soc Clin Oncol Educ Book 39: 147-164, 2019.
73. Nowicki TS, Hu-Lieskovan S and Ribas A: Mechanisms of resistance to PD-1 and PD-L1 blockade. Cancer J 24: 47-53, 2018.
74. Saleh R and Elkord E: Acquired resistance to cancer immunotherapy: Role of tumor-mediated immunosuppression. Semin Cancer Biol 65: 13-27, 2020.
75. Haratani K, Yonesaka K, Takamura S, Maenishi O, Kato R, Takegawa N, Kawakami H, Tanaka K, Hayashi H, Takeda M, *et al*: U3-1402 sensitizes HER3-expressing tumors to PD-1 blockade by immune activation. J Clin Invest 130: 374-388, 2020.
76. Arasanz H, Zuazo M, Bocanegra A, Gato M, Martínez-Aguillo M, Morilla I, Fernández G, Hernández B, López P, Alberdi N, *et al*: Early detection of hyperprogressive disease in non-small cell lung cancer by monitoring of systemic T cell dynamics. Cancers (Basel) 12: 344, 2020.
77. Hirsch L, Zitvogel L, Eggermont A and Marabelle A: PD-Loma: A cancer entity with a shared sensitivity to the PD-1/PD-L1 pathway blockade. Br J Cancer 120: 3-5, 2019.
78. Kim HAJ, Zeng PYF, Shaikh MH, Mundi N, Ghasemi F, Di Gravio E, Khan H, MacNeil D, Khan MI, Patel K, *et al*: All HPV-negative head and neck cancers are not the same: Analysis of the TCGA dataset reveals that anatomical sites have distinct mutation, transcriptome, hypoxia, and tumor microenvironment profiles. Oral Oncol 116: 105260, 2021.
79. Ahmadinejad F, Bos T, Hu B, Britt E, Koblinski J, Souers AJ, Leverson JD, Faber AC, Gewirtz DA and Harada H: Senolytic-mediated elimination of head and neck tumor cells induced into senescence by cisplatin. Mol Pharmacol 101: 168-180, 2022.